Sodium-Ion Batteries

DOI: 10.1002/anie.201206854

A Superior Low-Cost Cathode for a Na-Ion Battery**

*Long Wang, Yuhao Lu, Jue Liu, Maowen Xu, Jinguang Cheng, Dawei Zhang, and John B. Goodenough**

A global priority is the development of low-cost, efficient storage of off-peak electric power and of electrical energy generated by energy sources other than fossil fuels (e.g. wind, solar, nuclear).[1] The rechargeable battery offers efficient electrical energy storage (EES), but the Li-ion battery used in hand-held devices is too expensive for large-scale EES. Unlike Li, Na is readily available worldwide and therefore much less costly than Li. However, the existing Na/S[2] and Zebra ($Na/NiCl_2$)[3] batteries are operating on molten electrodes at 250 to 350 °C. Therefore, there is a huge incentive to develop a room-temperature rechargeable, low-cost Na-ion battery (SIB) of high energy density capable of discharge/charge at a high rate.

To date, room-temperature rechargeable batteries have used as cathode oxide hosts into/from which the working ion, H^+ or Li^+, can be inserted/extracted reversibly over a limited solid-solution range. These two working ions are able to be mobile guests in a host having a close-packed oxide-ion array. However, Na^+ is too large to be sufficiently mobile in a host with close-packed oxide ions; it needs a host framework with a larger interstitial space. Although Na^+ is stable coordinated by 12 oxide ions in an oxoperovskite, for example, the Na_xWO_3 bronze, too high an activation energy is required for Na^+ transfer between these sites across a shared face coordinated by four oxide ions. The O-2p orbitals that σ bond to the Na impede its motion. Replacement of the O^{2-} ions by $(C{\equiv}N)^-$ ions weakens bonding to the Na; the activation energy for Na^+ transfer is, therefore, strongly reduced, which makes attractive exploration of hexacyanoperovskites as cathode hosts for a rechargeable SIB. We report a synthesis route for a sodium manganese hexacyanoferrate (NMHFC) containing low-cost cations, and we demonstrate that the NMHFC provides a promising high-rate performance as the cathode of a SIB of high specific energy density and efficient EES.

Prussian blue and its analogues were investigated as hosts for alkali ions several years ago,[4] but that work received little attention. Cui and co-workers have recently reported stable Na^+ cyclability into potassium copper hexacyanoferrate in an aqueous electrolyte,[5] but an aqueous electrolyte limits the stable voltage of a rechargeable battery to 1.5 V. Therefore, we have chosen to investigate the hexacyano-perovskites in a non-aqueous electrolyte. We have reported the activities versus Na^+/Na^0 of $KMFe(CN)_6$ with M = Fe, Co, Ni, Mn, Zn; high-spin $M = Mn^{II}$ showed a reversible plateau at 3.82 and 3.56 V,[6] respectively, on charge and discharge. We report herein removal of the Na^+ ion for a SIB to obtain a 3.4 V cathode in a Na half-cell with rhombohedral $Na_{1.72}MnFe(CN)_6$ (NMHFC-1) and compare the performance with that of a cubic $Na_{1.40}MnFe(CN)_6$ (NMHFC-2).

The molar Na:Fe:Mn ratios of the sodium manganese hexacyanoferrates were obtained by inductively coupled plasma (ICP) analysis. All the metal atoms were normalized to the Mn content; the molar ratios were calculated to be 1.72:0.99:1.00 and 1.40:0.97:1.00 for NMHFC-1 and NMHFC-2, respectively. The NMHFCs with higher Na content require a higher Na^+ content in the water solution during sample preparation. Thermogravimetric analysis (TGA) from room temperature to 800 °C (see Figure S1 in the Supporting Information) indicates considerable water in the as-prepared compounds. Much of the water is adsorbed at the surface, but some may be absorbed into Na vacancies. The water content of NMHFC-1 was 12 wt%, of NMHFC-2 was 17 wt%. It is notable that the samples darken slightly from white on drying, which indicates that they are oxidized by the loss of water. The white color is expected for Mn^{II} and Fe^{II}, which would require H_3O^+ located in the Na-site vacancies; loss of H_3O^+ on drying would oxidize the samples and create vacancies for Na^+ mobility.

Since the Mn and Fe are coordinated by different atoms of the $(C{\equiv}N)^-$, Mn by N and Fe by C, the Fe ions are in a low-spin state while the Mn are in a high-spin state. Several different pairs of valence states are possible: Fe^{II}-CN-Mn^{II}, Fe^{III}-CN-Mn^{II}, Fe^{II}-CN-Mn^{III}, and Fe^{III}-CN-Mn^{III}. Figure 1a shows the Raman spectra between 2000 and 2300 cm^{-1}. Three peaks near 2090, 2130 and 2180 cm^{-1} have been observed. All these peaks can be assigned to the $(C{\equiv}N)^-$ group;[7] they reflect the bonding of the $(C{\equiv}N)^-$ ion to the transition-metal ions in different valence states.[7b] Two peaks at 2084 cm^{-1} and 2126 cm^{-1} have been observed from NMHFC-1 that can be attributed to the mixture of Fe^{II}-CN-Mn^{II} and Fe^{II}-CN-Mn^{III}. These two peaks shift to higher wavenumber in NMHFC-2

[*] L. Wang,[+] Y. H. Lu,[+] M. W. Xu, J. G. Cheng, Prof. J. B. Goodenough
Material Science and Engineering Program and Texas Materials Institute, The University of Texas at Austin
Austin, TX 78712 (USA)
E-mail: jgoodenough@mail.utexas.edu

J. Liu
Chemistry Department, State University of New York at Stony Brook
Stony Brook, NY 11794 (USA)

D. W. Zhang
School of Chemical Engineering, Hefei University of Technology
Hefei 230009 (P.R. China)

[+] These authors contributed equally to this work.

[**] We acknowledge Dr. Hengxing Ji for Raman spectra, Dr. Il Tae Kim for ICP analysis, and Dr. Sebastian Larregola for helpful discussions. M.X. is founded by the National Natural Science Foundation of China (No. 21063014).

Supporting information for this article is available on the WWW under http://dx.doi.org/10.1002/anie.201206854.

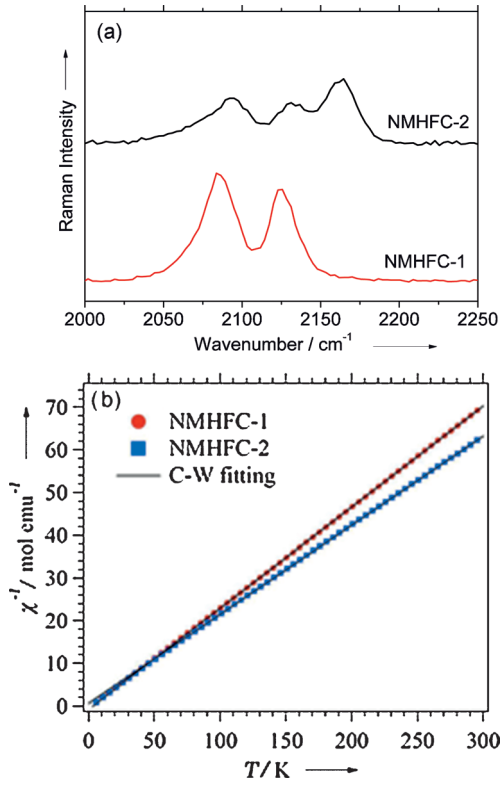

Figure 1. a) Raman spectra and b) magnetic susceptibility versus temperature of NMHFCs.

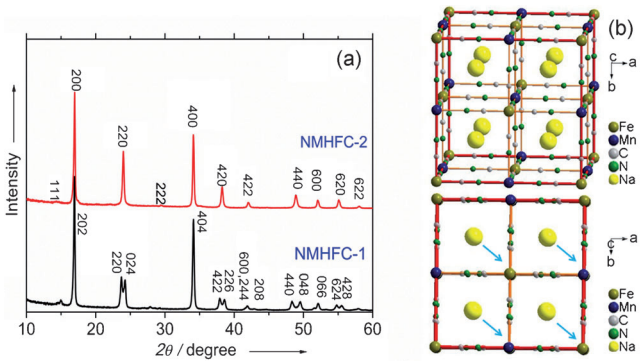

Figure 2. a) XRD patterns of NMHCs. b) Crystal structures of cubic NMHFC (upper) and the alkali-ion displacement along a [111] resulting in rhombohedral symmetry (lower).

because the average valence state of the transition metals is higher in NMHFC-2 than in NMHFC-1. Moreover, in NMHFC-2 an additional strong peak appears at 2180 cm^{-1} that is assigned to Fe^{III}-CN-Mn^{II}. Thus, it can be concluded that there is a certain amount of Mn^{III} in NMHFC-1 while almost all the Fe remain as Fe^{II}. On the other hand, part of the Fe^{II} has been oxidized to Fe^{III} in NMHFC-2 and only a weak signal of Mn^{III} has been observed from the Raman spectra.

In our former work, we have discussed the influence on voltage of the spin state of the transition metals in the Prussian blue analogues; differences in the energies of low and high-spin states can lead to different potentials of the same redox couple.[6] Thus, it is important to confirm the spin state of Mn and Fe in our NMHFCs. Figure 1b shows the magnetic susceptibility (χ) of NMHFCs against temperature. Both samples exhibit paramagnetic behavior from low temperature until room temperature, and there is no phase transition observed in this temperature range. The calculated effective magnetic moments (μ_{eff}) of NMHFC-1 and NMHFC-2 are 5.8 and 6.2 μ_B per formula, respectively. The smaller μ_{eff} of NMHFC-1 indicates the presence of some Mn^{III} ($S=2$) to give $Mn^{II}_{1-x}Mn^{III}_{x}Fe^{II}$ whereas the larger μ_{eff} of NMHFC-2 indicates the presence of some low-spin Fe^{III} ($S=1/2$) to give $Mn^{II}Fe^{II}_{1-x}Fe^{III}_{x}$ consistent with the Raman spectra. These data also show that the low-spin Fe^{III}/Fe^{II} and high-spin Mn^{III}/Mn^{II} couples have comparable energies with the NMHFC-1 phase stabilizing the Mn^{III}/Mn^{II} couple relative to the Fe^{III}/Fe^{II} couple.

The X-ray diffraction (XRD) patterns of Figure 2a show that the as-prepared NMHFC-1 sample is rhombohedral (space group $R\bar{3}m$) with $a=b=15.02$ Å and $c=17.80$ Å whereas the NMHFC-2 sample is cubic ($Fm\bar{3}m$) with $a=10.49$ Å. A similar structural change has been reported within $Na_{1.32}Mn[Fe(CN)_6]_{0.83}\cdot 3.6H_2O$ where a high-temperature cubic phase becomes rhombohedral below $T_t=280$ K.[8] The double-perovskite ordering of both the anion orientations and the cations introduces a rhombohedral site symmetry along each of the four [111] axes that would stabilize an alkali-ion displacement along a cubic [111] axis toward the more negative octahedral-site complex. The fourfold degeneracy of these displacements keeps the cubic phase at higher temperature and lower Na concentration, but a cooperative Na displacement at higher Na concentration reduces the crystal symmetry to rhombohedral, stabilizing the rhombohedral phase (Figure 2b). The larger the concentration of the alkali ions in the compound, the higher the temperature of transition from rhombohedral to cubic symmetry.

Moreover, the displacement of Na^+ ions toward the $Fe(CN)_{6/2}$ complex would stabilize a higher net positive charge on the Mn versus the Fe ions to shift the Fe^{III}/Fe^{II} couple to a Mn^{III}/Mn^{II} couple.

Figure 3a shows the voltage profiles of NMHFC/Na half-cells. NMHFC-1 shows a lower open-circuit voltage (OCV) of 3.27 V compared to NMHFC-2, which has an OCV of 3.34 V, consistent with the higher average valence state of the transition metals in NMHFC-2. Two plateaus have been observed during the charge (3.52 and 3.85 V) and discharge (3.27 and 3.57 V) in the first cycle, as was found in the cubic $KMnFe(CN)_6$.[6,9] The reactions occurring at low and high potential can be assigned to low-spin Fe^{III}/Fe^{II} and high-spin Mn^{III}/Mn^{II} redox couples, respectively. NMHFC-1 and NMHFC-2 show almost the same behavior during Na^+ extraction/insertion in the first cycle, indicating that the initial structural differences have no influence on the reaction potentials. Nevertheless, NMHFC-1 exhibits a higher reversible capacity than NMHFC-2, with an initial charge/discharge capacity of 143 and 134 mA h g^{-1}, respectively. As expected with a smaller initial Na^+ concentration, NMHFC-2 shows a higher discharge capacity (123 mA h g^{-1}) than charge (111 mA h g^{-1}), especially below 3.4 V where the reduction of

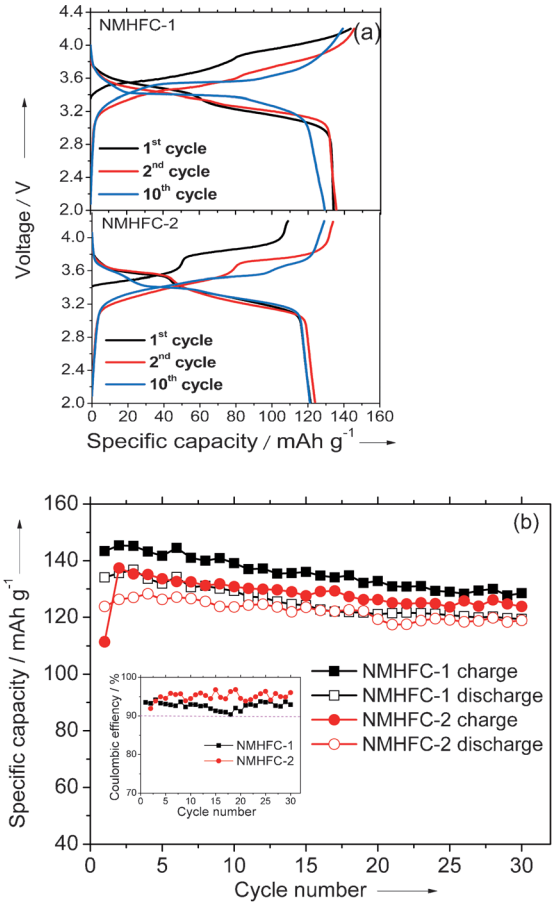

Figure 3. a) Voltage profiles at different cycles of NMHFCs/Na half cells. b) Charge/discharge capacity and coulombic efficiency (inset image) versus cycle number. All the cells were cycled between 2.0 to 4.2 V at a current density of 1/20 C (120 mA g^{-1} at 1 C).

Fe^{III} occurs on discharge. After the activation in the first charge process, the two plateaus drop to lower potentials in the subsequent charge process, indicating a decrease in the cell impedance. Interestingly, the voltage profiles of these sodium-ion cells change gradually from two-step curves into three-step curves. In the discharge curve of NMHFC-2, for example, the first slope above 3.4 V becomes shorter while another flat plateau occurs at 3.43 V that becomes longer as the Na insertion/extraction is repeated. This voltage plateau is higher than that of $Na_4Fe(CN)_6$ (3.34 V).[10] However, the overall discharge capacity stays the same. We have checked the ex-situ XRD patterns of NMHFC-1 electrodes discharged to 2.0 V after one and 50 cycles; no obvious structural change occurred except some split peaks become one broad peak (Figure S2). Nevertheless, the potential shift indicates that the relative redox energies of Mn^{III}/Mn^{II} and Fe^{III}/Fe^{II} couples, which are located separately before cycling, shift gradually with Na^+ extraction/insertion and finally overlap (Figure S3). Therefore, the final redox potential is higher than the original Fe^{III}/Fe^{II} couple but lower than that of the Mn^{III}/Mn^{II} couple.

One of the biggest challenges for a Na-ion battery is the cycle life of the cathode material.[11] We have already demonstrated that Prussian blue $KFeFe(CN)_6$ with an open framework is quite stable in a carbonate electrolyte during Na^+ insertion/extraction.[6] Figure 3b shows the cycling performance of NMHFC/Na half-cells. NMHFC-1 shows a fast capacity fade during the first several cycles; but it becomes more stable after 10 cycles, showing a discharge capacity as high as 130 mA h g^{-1} that retains 121 mA h g^{-1} after 30 cycles at a current density of 1/20 C. Meanwhile, NMHFC-2 shows a stable capacity with negligible capacity fade and retains 96 % of the original capacity even after 30 cycles. The cell with NMHFC-1 was also cycled under a higher current density of 0.5 C for 50 cycles and then disassembled to check for dissolution of metal ions in the electrolyte. No Fe or Mn was found on the separator by X-ray energy dispersive spectroscopy (EDS), indicating the NMHFC is quite stable at room temperature even in the presence of Mn^{III}. The capacity fade is ascribed to a phase transition during Na^+ insertion/extraction. Figure S4a shows the ex-situ Raman of NMHFC-2 at the fully charged/discharged states in the first cycle. After full discharge to 2.0 V, the peak of Fe^{III} at 2180 cm^{-1} disappears while the relative intensity of the Mn^{III} peak at 2130 cm^{-1} becomes much stronger, and the spectrum is similar to that obtained from NMHFC-1 pristine powder. Also, the ex-situ XRD results in Figure S4b clearly indicate that NMHFC-1 undergoes a rhombohedral-cubic phase transition when charged to 4.2 V and becomes rhombohedral again when discharged to 2.0 V in the first cycle. Nevertheless, a NMHFC with a stable reversible capacity of more than 120 mA h g^{-1} and a high voltage of ca. 3.4 V is a promising cathode for a SIB.

Figure 4 shows the discharge curves of NMHFC-1 at various current densities. It exhibits excellent rate capability. Even at an ultra-high discharge rate of 40 C, it can still deliver

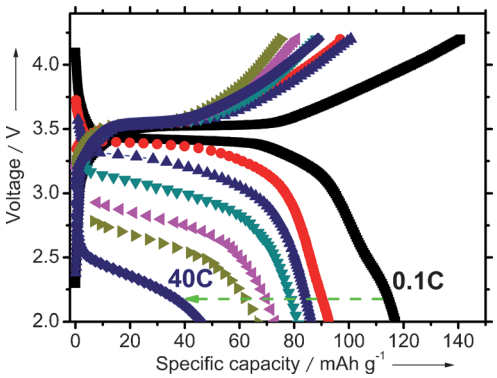

Figure 4. Charge/discharge curves of a NMHFC-1/Na half-cell at various current densities (follow the arrow by order of 0.1, 0.85, 3.5, 8.5, 17, 26, and 40 C, 120 mA g^{-1} at 1 C). The cell was cycled between 2.0 to 4.2 V at 0.1 C for 30 cycles before the rate test.

a capacity of 45 mA h g^{-1}. Since the as-prepared NMHFCs are poor electronic conductors, the rate capability can be further improved by forming a composite with carbon. Although the specific capacity of NMHFC is lower than that of some of the LIB cathodes ($LiCoO_2$, $LiFePO_4$, $LiNi_{1/3}Co_{1/3}Mn_{1/3}O_2$, …), its excellent rate capability ensures the high power density required by power tools and stationary energy storage. In

summary, sodium manganese hexacyanoferrates with two structures can be synthesized at room temperature. The sodium-ion concentration in the aqueous solution during precipitation has a strong influence on the composition and structure of the final product, resulting in different reversible capacity and cycling performance. With higher Na^+ concentration, a cooperative Na^+ displacement along a single [111] direction induces a transition from cubic to rhombohedral symmetry; this phase transition is reversible on cycling the Na^+ concentration. NMHFC-1 with an initial rhombohedral structure exhibits a reversible capacity of 134 $mA\,h\,g^{-1}$ and retains 120 $mA\,h\,g^{-1}$ after 30 cycles. The high power density and high rate capability of NMHFC-1 make it a promising cathode material for rechargeable SIBs.

Received: August 23, 2012
Revised: December 7, 2012
Published online: January 14, 2013

Keywords: cathode materials · hexacyanoferrates · sodium-ion battery

[1] a) B. Dunn, H. Kamath, J. M. Tarascon, *Science* **2011**, *334*, 928 – 935; b) Z. G. Yang, J. L. Zhang, M. C. W. Kintner-Meyer, X. C. Lu, D. W. Choi, J. P. Lemmon, J. Liu, *Chem. Rev.* **2011**, *111*, 3577 – 3613.

[2] X. C. Lu, G. G. Xia, J. P. Lemmon, Z. G. Yang, *J. Power Sources* **2010**, *195*, 2431 – 2442.

[3] a) R. J. Bones, D. A. Teagle, S. D. Brooker, F. L. Cullen, *J. Electrochem. Soc.* **1989**, *136*, 1274 – 1277; b) J. L. Sudworth, *J. Power Sources* **2001**, *100*, 149 – 163.

[4] a) A. Eftekhari, *J. Power Sources* **2004**, *126*, 221 – 228; b) N. Imanishi, T. Morikawa, J. Kondo, Y. Takeda, O. Yamamoto, N. Kinugasa, T. Yamagishi, *J. Power Sources* **1999**, *79*, 215 – 219.

[5] a) C. D. Wessells, M. T. McDowell, S. V. Peddada, M. Pasta, R. A. Huggins, Y. Cui, *ACS Nano* **2012**, *6*, 1688 – 1694; b) C. D. Wessells, S. V. Peddada, M. T. McDowell, R. A. Huggins, Y. Cui, *J. Electrochem. Soc.* **2012**, *159*, A98 – A103; c) C. D. Wessells, R. A. Huggins, Y. Cui, *Nat. Commun.* **2011**, *2*, 550.

[6] Y. H. Lu, L. Wang, J. G. Cheng, J. B. Goodenough, *Chem. Commun.* **2012**, *48*, 6544 – 6546.

[7] a) T. Suemoto, K. Ohki, R. Fukaya, M. Nakajima, H. Tokoro, S. Ohkoshi, *J. Lumin.* **2009**, *129*, 1775 – 1778; b) E. J. M. Vertelman, T. T. A. Lummen, A. Meetsma, M. W. Bouwkamp, G. Molnar, P. H. M. van Loosdrecht, P. J. van Koningsbruggen, *Chem. Mater.* **2008**, *20*, 1236 – 1238.

[8] S. I. Ohkoshi, H. Tokoro, M. Utsunomiya, M. Mizuno, M. Abe, K. Hashimoto, *J. Phys. Chem. B* **2002**, *106*, 2423 – 2425.

[9] Y. Mizuno, M. Okubo, D. Asakura, T. Saito, E. Hosono, Y. Saito, K. Oh-ishi, T. Kudo, H. S. Zhou, *Electrochim. Acta* **2012**, *63*, 139 – 145.

[10] J. Qian, M. Zhou, Y. Cao, X. Ai, H. Yang, *Adv. Energy Mater.* **2012**, *2*, 410 – 414.

[11] a) S. W. Kim, D. H. Seo, X. H. Ma, G. Ceder, K. Kang, *Adv. Energy Mater.* **2012**, *2*, 710 – 721; b) J. Barker, M. Y. Saidi, J. L. Swoyer, *Electrochem. Solid-State Lett.* **2003**, *6*, A1 – A4.

